Role of doped ZnO nanoparticles as polymer chain segmental motion exciter in PVA-ZnO nanocomposites investigated by dielectric relaxation spectroscopy

Shobhna Choudhary*, Ram J. Sengwa*

Dielectric Research Laboratory, Department of Physics, Jai Narain Vyas University, Jodhpur 342 005, India

*Corresponding author: E-mail: shobhnachoudhary@rediffmail.com

Received: 28 March 2016, Revised: 13 September 2016 and Accepted: 21 September 2016

DOI: 10.5185/amp.2017/507
www.vbripress.com/amp

Abstract

The dielectric and electrical spectra of solution cast prepared nanocomposite films comprising poly(vinyl alcohol) (PVA) as polymer matrix and zinc oxide (ZnO) as inorganic nanofiller (PVA–*x* wt% ZnO (*x* = 0, 1, 3 and 5)) have been investigated in the frequency range from 20 Hz to 1 MHz. Anomalous increase is observed in real part of complex permittivity with increase of ZnO concentration, whereas relaxation peak corresponding to PVA chain segmental motion is appeared in the intermediate frequency region of dielectric loss tangent and the loss part of electric modulus spectra of the nanocomposites. These results confirm that the interaction of ZnO nanoparticles with hydroxyl groups of PVA acts as exciter for polymer chain segmental dynamics in the nanocomposites. The temperature dependent dielectric investigations on PVA–3 wt% ZnO film reveal that the dielectric polarization and chain segmental dynamics increase with the increase of temperature. The dielectric relaxation and conductivity activation energies values of the film are determined from the Arrhenius relation, which are found equal. The X-ray diffraction study confirms that the crystalline phase of PVA matrix abruptly reduces with doping of only 1 wt% ZnO which suggests that the interaction of polymer-nanoparticles significantly alter the hydrogen bonded crystalline structure of pristine PVA matrix. The dielectric and electrical results showed that these nanodielectrics are potentially useful as an electrical insulation material for various electronic devices.

Keywords: Nanodielectric, dielectric properties, electrical conductivity, X-ray diffraction, polymer dynamics.

Introduction

Polymeric nanocomposites (PNCs) have established as technologically novel materials due to their improved electrical, optical, mechanical, thermal and magnetic properties **[1–8]**. These materials are prepared by incorporating a small amount of inorganic nanoparticles into a suitable polymer matrix using solution cast, melt compounding and in-situ synthesis methods. The preparation and characterization of PNCs have been the subject of intense research because of their ability to combine the useful properties of both polymer and inorganic nanofiller. They include major advantages of processability, flexibility, ductility and electrical insulation of the polymer, and rigidity, thermal stability, barrier and flame retardancy of the nanofiller. The interactions between polymer and nanofiller result in improvement of their useful properties as required in the emerging technological applications of such advanced materials.

Among the various kind of PNCs, poly(vinyl alcohol) (PVA)–zinc oxide (ZnO) nanocomposites have attracted large academic, industrial and technological interest **[9–20]**. PVA is a hydrophilic, non-toxic, biocompatible and hot water soluble polymer. High optical transparency, good chemical resistance and high electrical insulating behaviour of pristine PVA film make it the most suitable as binder, substrate and insulator in fabrication of various electronic devices **[21–23]**. In addition to these applications, it also has many other technological, pharmaceutical and biomedical applications **[24–26]**. In regards to inorganic nanoparticles, ZnO has gained more attention due to its non-toxicity and highly stable physical and chemical properties. It is a II-IV compound semiconductor of a wide direct band gap (3.22 eV at 300 K) and high excitation binding energy (60 meV; which is larger than the thermal energy at room temperature) **[9]**. Beside these, the superior electronic and optical properties of ZnO result its promising applications in optoelectronic devices and sensors (blue light emitter, transparent conductor, dye-sensitized solar cell, piezo-electric

material, gas sensing varistors, transparent thin film transistor, lasers, etc.) **[10–14,20,27, 28]**. The interfacial interaction between PVA chain and ZnO nanoparticles which in turn affects the PVA chain mobility in the interfacial area and it is the most decisive factor governing the various properties of PVA–ZnO nanocomposites. The hydrogen bond interaction between hydroxyl groups (functional group) of PVA repeating units and oxygen atoms of ZnO nanoparticles causes the formation of PVA–ZnO nanocomposite when prepared by aqueous solution casting method.

Although, extensive work on mechanical, thermal, optical, morphology and structural properties of PVA–ZnO nanocomposites has already been explored **[10–20,27,28]**, but their dielectric and electrical properties were merely attempted **[9,16–19]**. Therefore, in this paper the dielectric dispersion spectra and relaxation process of PVA–ZnO nanocomposites have been investigated by dielectric relaxation spectroscopy (DRS). The effect of ZnO nanofiller on the chain segmental dynamics of PVA is explored by simultaneous analysis of the complex permittivity and complex electric modulus spectra of the nanocomposites. Further, complex ac electrical conductivity and impedance behaviour of PVA–ZnO nanocomposites have also been reported and discussed in view of their suitability as flexible type nanodielectric material **[2]**.

Experimental

Materials

PVA (M_w = 77000 g mol^{-1}) of laboratory regent and ZnO nanopowder of particles sizes less than 100 nm were purchased from Loba Chemie, India, and Sigma-Aldrich, USA, respectively.

The nanocomposites of PVA dispersed with *x* wt% amount of ZnO (*x* = 0, 1, 3 and 5 wt% amounts of ZnO to the weight of PVA amount) were prepared by solution casting method. For each sample, initially 1 g of PVA was dissolved in 20 ml double distilled deionized water by slow heating up to 90 °C. The required amount of ZnO for each sample was firstly dispersed in 10 ml water. After that the PVA and ZnO aqueous solutions were mixed and magnetically stirred for 1 h to obtain a homogenous viscous solution. This solution was cast on to a poly propylene petri dish and was kept to dry at room temperature for few days which resulted highly stable and flexible type nanocomposite film. Different ZnO concentrations nanocomposite films were prepared simultaneously by following the same procedure. Finally, the PVA–*x* wt% ZnO films were dried in vacuum oven at 40 °C for 24 h to remove the solvent traces and after that these films were used for their structural and dielectric characterization.

Measurements

The X-ray diffraction (XRD) patterns of the ZnO nanopowder and PVA–*x* wt% ZnO films were recorded in reflection mode at a scan rate of 0.05 degree/s using a PANalytical X′pertPro MPD diffractometer of Cu-Kα radiation. The X'pert pro® software was used for analysis of the XRD patterns of these materials.

DRS measurements of the PNC films were carried out by employing an Agilent technologies 4284A precision LCR meter and 16451B solid dielectric test fixture in the frequency range of 20 Hz to 1 MHz at fixed temperature 30 °C. The DRS measurements of PVA–3 wt% ZnO film have also been carried out at temperatures 40, 50 and 60°C. For temperature dependent measurements the dielectric test fixture loaded with PNC film was placed in the cavity of hot oven and the temperature of the cavity was controlled using microcontroller. The frequency dependent values of capacitance C_p, resistance R_p and loss tangent (dissipation factor) tanδ were measured and the same were used for evaluation of dielectric and electrical spectra of the PNC films. The spectra of complex dielectric function $\varepsilon^*(\omega) = \varepsilon' - j\varepsilon''$, alternating current (ac) electrical conductivity $\sigma^*(\omega) = \sigma' + j\sigma''$, electric modulus $M^*(\omega) = M' + jM''$ and complex impedance $Z^*(\omega) = Z' - jZ''$ of the PNC films were determined using the C_p, R_p and tanδ dependent equations described in detail elsewhere **[6,29]**.

Results and discussion

XRD patterns and structural analysis

XRD patterns of ZnO nanopowder and PVA–*x* wt% ZnO nanocomposite films are shown in **Fig. 1(a)**. The ZnO has various sharp peaks corresponding to different diffraction planes which are marked in the figure. These diffraction peaks positions and intensities are found in good agreement as reported in literature **[9,10,14]**, which confirms the typical hexagonal wurtzite structure of ZnO (space group: $P6_3mc$, JCPDS No. 36–1454). Further, the strong and sharp diffraction peaks reveal highly well-crystallized structures of the ZnO material. The values of *d*-spacing corresponding to these crystalline peaks were determined by the Bragg's relation $\lambda = 2d\sin\theta$, where λ is the wavelength of X-ray radiation (λ = 1.5406 Å), *d* is the spacing between diffractional lattice planes (*hkl*) and θ is the measured diffraction angle (Bragg's angle) of the respective peaks. The values of 2θ corresponding to *hkl* planes and d_{hkl} of ZnO nanoparticles are listed in **Table 1**. The value of mean crystallite size *L* in the direction perpendicular to various (*hkl*) planes of the ZnO nanoparticles was evaluated by Scherrer's equation $L = \lambda k/\beta\cos\theta$, where $k = 0.94$ is a constant and β is full width at half maximum (FWHM) (i.e. the broadening of peak at half-height expressed in radians of 2θ which is obtained by width measured in 2θ degrees and then multiplied by π/180). The values of FWHM and L_{hkl} along with peak intensities *I* and relative peak *RI* intensities with respect to the maximum intensity peak (2θ = 36.28°) of ZnO nanoparticles are given in **Table 1**. The average crystallite size of ZnO was found 35 nm. The comparative sizes of crystallites (35 nm) and nanoparticles (100 nm) suggest that one grain in ZnO nanoparticle consists of approximately three crystallites.

Table 1. Values of Bragg's angle 2θ, different planes *hkl*, basal spacing d_{hkl}, full width at half maximum $FWHM_{hkl}$, crystallite size L_{hkl}, peak intensity (counts) *I* and relative intensity *RI* with respect to maximum intense peak (2θ = 36.28°) of ZnO nanoparticles.

2θ (degree)	*hkl* planes	d_{hkl} (nm)	$FWHM_{hkl}$ × 10^3 (rad)	L_{hkl} (nm)	*I* (counts)	*RI* (%)
31.79	100	0.281	3.700	40.69	7122	62.6
34.45	002	0.260	3.508	43.22	4891	43.0
36.28	101	0.247	3.875	39.33	11378	100.0
47.57	102	0.191	4.468	35.42	2262	19.9
56.63	110	0.162	5.061	32.50	3635	31.9
62.88	103	0.148	5.341	31.78	2857	25.1
66.39	200	0.141	5.672	30.51	455	4.0
67.97	112	0.138	5.812	30.05	2324	20.4
69.11	201	0.136	5.969	29.46	1116	9.8

The broad and intense peak in XRD pattern of pure PVA film at 2θ = 19.59° reveals its semi crystalline structure as reported earlier **[13,23,30]**. This peak is corresponding to concurrent crystal reflections 101 and $10\bar{1}$ of the PVA. The crystalline phases in pristine PVA network are formed due to intermolecular H-bonding between hydroxyl groups of neighbouring chains **[23]**. The PVA film also has a broad and diffuse peak at 2θ = 41.97° related to its typical structural behaviour. These peaks of PVA are found in good agreement of literature value (JCPDS No. 53–1487). When 1 wt% ZnO amount is dispersed in PVA matrix, the PVA peak position changed very slightly (i.e. 0.4° from 19.59° to 19.99°) with a huge decrease in intensity (i.e. almost half of the pristine PVA peak intensity). Further, a little but anomalous variation in the intensities of this PVA peak with the change of ZnO concentration up to 5 wt% is also observed for these nanocomposites. The decrease of crystalline peak of PVA with addition of ZnO reveals that there is formation of hydrogen bonds between –OH groups of PVA with the oxygen atoms which exist on the ZnO surface nanoparticles, and confirm the surface passivation of PVA on ZnO nanoparticles as discussed earlier **[20,31]**. Due to PVA and ZnO interactions, the intermolecular H-bonding between PVA chains reduces, and thereby leads to decrease of PVA crystallinity on addition of ZnO nanoparticles.

Table 2. Values of Bragg's angle 2θ, basal spacing *d*, full width at half maximum FWHM, crystallite size *L*, peak intensity (counts) *I* and relative intensity *RI* with respect to pristine PVA peak (2θ = 19.59°) of PVA–*x* wt% ZnO nanocomposites.

x	2θ (degree)	*d* (nm)	FWHM × 10^3 (rad)	*L* (nm)	*I* (counts)	*RI* (%)
0	19.59	0.4528	34.75	4.23	2969	100
1	20.01	0.4434	37.93	3.88	1641	55.3
3	19.99	0.4438	35.90	4.10	1619	54.5
5	19.98	0.4440	36.70	4.01	1573	53.0

The XRD parameters of PVA in the PVA–*x* wt% ZnO films are reported in **Table 2**. **Fig. 1(b)** shows that the *L* and *RI* values of PVA–*x* wt% ZnO vary non-linearly with increase in concentration of ZnO in PVA matrix. It is found that the *L* of PVA increases whereas *RI* decreases with increase of ZnO concentration confirming the formation of bigger size crystallites with decrease of total crystalline phase of PVA in the nanocomposites. Further, the PVA–ZnO films exhibit diffraction peaks of both the PVA and ZnO structures which conclude the formation of PVA–ZnO nanocomposite material. Furthermore, inset of **Fig. 1(a)** reveal that the intensities of ZnO peaks increase with the increase of ZnO concentration in the PVA–ZnO films but these peaks positions are unchanged, which suggest that ZnO structure remains unaltered upon the interactions between PVA and ZnO. The increase of ZnO peaks intensity is also due to increase of ZnO content in the nanocomposites which is in good agreement with the earlier findings **[13, 19]**.

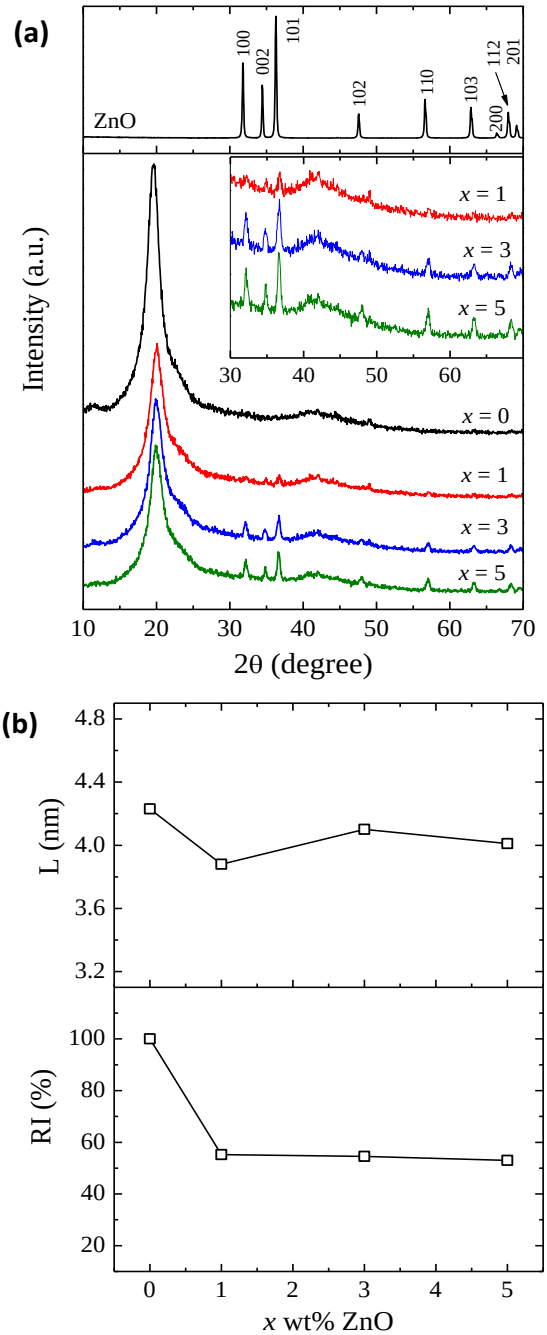

Fig. 1. (a)XRD patterns of ZnO nanopowder and PVA–*x* wt% ZnO nanocomposite films and (b) ZnO concentration dependent crystallite size (*L*) and relative intensity (*RI*) of PVA–*x* wt% ZnO nanocomposite films.

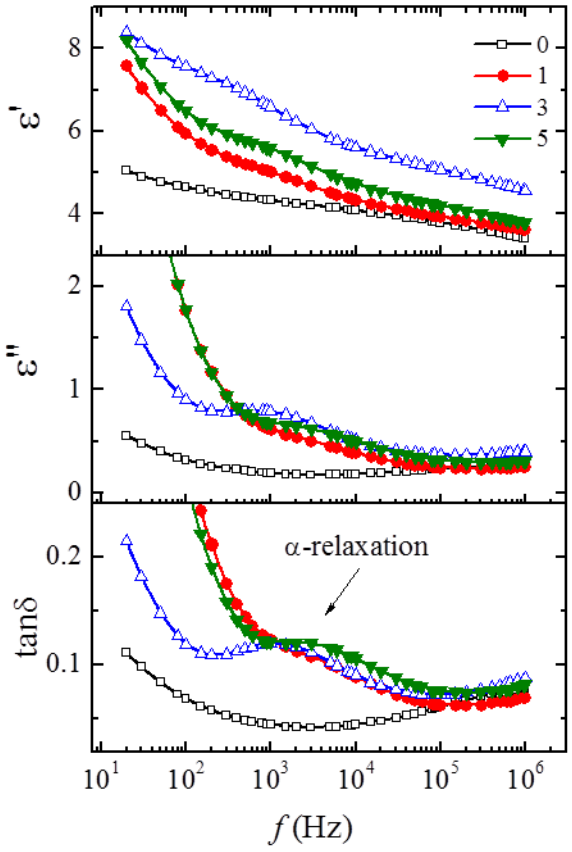

Fig. 2. Frequency dependent real part ε′ and loss part ε″ of the complex dielectric function, and loss tangent tanδ of PVA–*x* wt% ZnO nanocomposite films at 30 °C.

Effect of ZnO concentration on dielectric behavior of PNC films

Dielectric dispersion spectra

Fig. 2 shows the frequency dependent real part ε′ and loss part ε″ of complex dielectric function (permittivity) and also loss tangent (tanδ = ε″/ε′) of PVA–*x* wt% ZnO nanocomposites at 30 °C. It is found that ε′ values of these materials non-linearly decrease with the increase of frequency. The decrease of ε′ with increase in frequency is due to the fact that at low frequency the electric dipoles (or polymer chains) can follow slow varying the electric field but as the frequency increases they can no longer follow the fast-changing field and as a result of which, the ε′ values decrease. The frequency dependent ε′ values of pure PVA film are found in good agreement with the values reported earlier **[32]**. ZnO is a polar ceramic material of relatively high permittivity as compared to pristine PVA, and therefore, the ε′ values of the nanocomposites are also found higher. Further, the significant increase of ε′ values of PNCs at low frequencies can be attributed to the interfacial polarization which exhibits due to the difference in the permittivity values of the nanofiller and polymer matrix. The contribution of interfacial polarization on dielectric permittivity, particularly in the low frequency region, is a common phenomenon in PNC materials **[6–8,32–34]**.

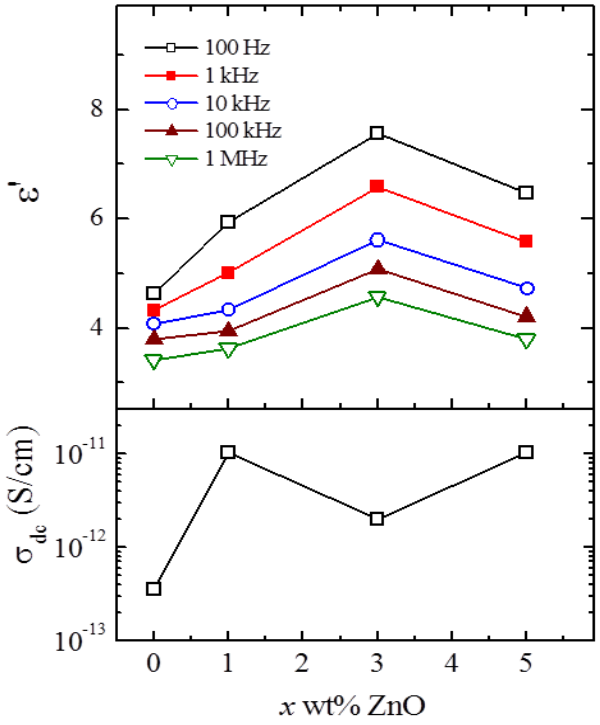

Fig. 3. ZnO concentration dependent ε′ and dc conductivity σ_{dc} values of PVA–*x* wt% ZnO nanocomposite films at 30 °C.

The variation of ε′ values with ZnO concentration at the fixed frequencies is shown in **Fig. 3**. This figure clearly confirms that the trend of variation in ε′values with increase of ZnO concentrations in the nanocomposite is identical at various fixed frequencies. It is also observed that, initially, the increase in ε′ with increase of ZnO concentration up to 3 wt% is definitely due to high ε′ value of ZnO, but the decrease in ε′ value at 5 wt% ZnO containing film confirms that there is huge disturbance in the ordered dipolar structures of PVA at higher ZnO concentration.

The ε″ and tanδ spectra of the nanocomposites exhibit the dielectric relaxation peak in the intermediate frequency region (**Fig. 2**), whereas pristine PVA does not exhibit such relaxation process over the examined frequency range. The gradual increasing tendency of ε″ and tanδ values of pristine PVA near the high frequency and also the low frequency edges of the spectra infer that PVA may have relaxation peaks beyond the present experimental frequency range. Thus, it is reasonable to suggest that the observed relaxation process in PNCs is due to nanoinclusions in PVA matrix. This relaxation process is attributed to local chain dynamics (α-relaxation) of PVA. These results confirm that the interaction of ZnO with PVA acts as exciter for polymer chain dynamics. Further, the relaxation time for this PVA chain dynamical process is higher for 3 wt% PNC and lower for 5 wt% PNC as compared to 1 wt% PNC which also suggests the anomalous behaviour of polymer-nanoparticle interaction strength with the increase of ZnO concentration at fixed temperature. The low frequency relaxation process may be attributed to the Maxwell-

Wagner-Sillars (MWS) interfacial polarization, whereas the high frequency relaxation process can be assigned to the dipolar orientation polarization in these composite materials, which seems beyond the present experimental frequency range.

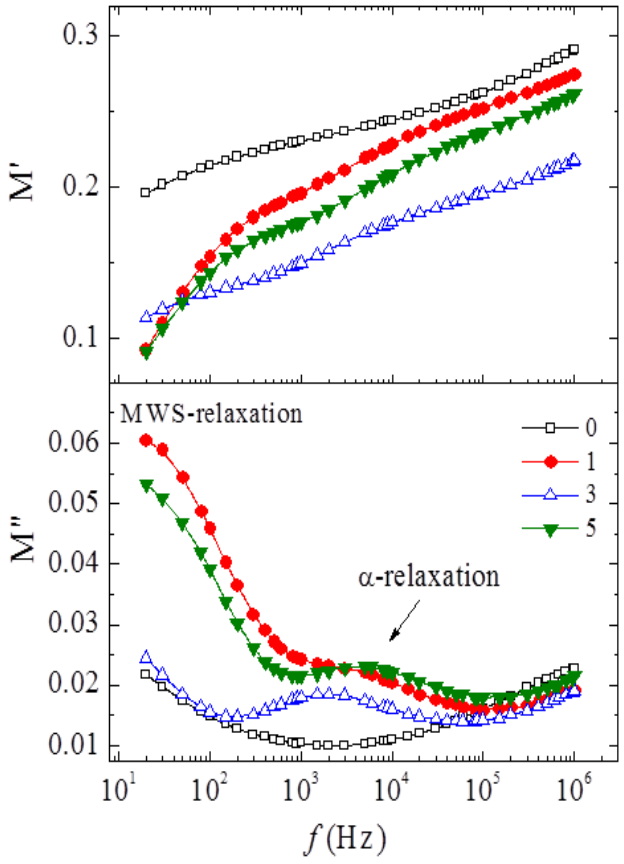

Fig. 4. Frequency dependent real part *M′* and loss part *M″* of complex electric modulus of PVA–*x* wt% ZnO nanocomposite films at 30 °C.

Electric modulus spectra

The complex electric modulus spectra of the PNC materials are studied in order to explore the bulk response of the material with nullifying the contribution of electrode polarization effect. The spectra of real part *M′* and loss part *M″* of electric modulus for PVA–*x* wt% ZnO nanocomposites at 30 °C are depicted in **Fig. 4**. It is found that *M′* values non-linearly increase with the increase of frequency, whereas *M″* spectra of these materials exhibit a relaxation process in the intermediate frequency region. This process matches with the relaxation processes observed in their ε″ and tanδ spectra which is definitely corresponding to PVA local chain motion. Further, for 1 wt% and 5 wt% ZnO filled nanocomposite films, the *M″* spectra seem to approaching the relaxation peak near lower frequency end which is an indication of the presence of MWS relaxation process as observed in the semicrystalline PVA below 10 Hz **[9]**. The MWS relaxation is attributed to the trapping of ionic charges at the interface of amorphous and the crystalline regions of the polymer network, and also due to accumulation of charges at the interface of different conductivity constituents in the polymeric nanocomposites. The comparative study of *M″* spectra of the PNC films reveals that the MWS relaxation process is also influenced by the added concentration of ZnO nanofiller in the PVA matrix.

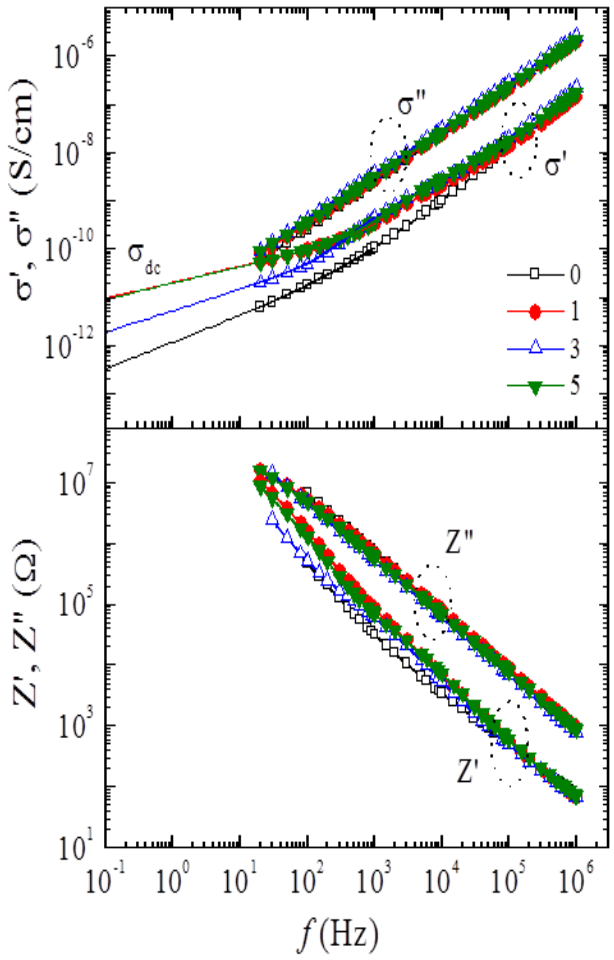

Fig. 5. Frequency dependent real part σ′ and loss part σ″ of the complex ac electrical conductivity, and real part *Z′* and reactive part *Z″* of complex impedance of PVA–*x* wt% ZnO nanocomposite films at 30 °C.

Ac conductivity and impedance spectra

The spectra of real part σ′ and loss part σ″ of the complex ac electrical conductivity of PVA–*x* wt% ZnO nanocomposites at 30 °C are shown in upper layer of **Fig. 5**. It is found that the σ′ values in high frequency region and σ″ values over the entire frequency range increase linearly with increase of frequency. At low frequencies, long-range transport of charges occurs through the semiconducting islands in the insulating PVA matrix, but as the frequency increases the localized charge carries contribution increases and hence the ac conductivity increases linearly. Further the frequency dependent σ′ values are found lower than that of the corresponding σ″ values of these materials. The σ′ values of these nanocomposites are lower than 10^{-10} S/cm at 20 Hz, and with increase of frequency it attains the values

higher than 10^{-7} S/cm at 1 MHz. The dispersion behaviour of σ′ spectra of pristine PVA is found in good agreement with the earlier study **[33]**. The non-linear decrease of σ′ values below 1 kHz indicates that the conductivity tends to acquire limiting values corresponding to the dc conductivity σ_{dc}. Therefore, the σ_{dc} values of these nanocomposite films were estimated by interpolation of the σ′ spectra with $f \rightarrow 0$ as shown in the figure. The σ_{dc} of pristine PVA is found 3.54×10^{-13} S/cm whereas the PNC films have one to two orders of magnitude higher σ_{dc} values as compared to that of the PVA matrix, at 30 °C. Further, 1 and 5 wt% ZnO loaded PNC films have equal σ_{dc} values and these are about one order of magnitude higher than that of 3 wt% ZnO added PNC film.

The spectra of real part Z' and reactive part Z'' of complex impedance of the PVA–*x* wt% ZnO films at 30 °C are also shown in lower layer of **Fig. 5**. It is observed that both the Z' and Z'' decrease almost linearly with increase of frequency, and shows a little variation with ZnO concentrations in these PNC films. The high magnitude of Z'' as compared to the Z' at same frequency suggests the dominant capacitive behaviour of these materials. Further, the low frequency impedance values of these nanodielectric materials are of the order of several MΩ which confirm their high electrical insulation property, and therefore these nanodielectrics confirm their suitability as insulator for audio frequency electric field operating microelectronic devices.

Effect of temperature on dielectric behaviour of PNC film

Fig. 6 presents the ε′, ε″ and tanδ spectra of PVA–3 wt% ZnO nanocomposite film at different temperatures. It is observed that as the temperature of the film increases the values of the ε′ also increase. To understand the increasing trend of ε′ with temperature, the ε′ values at fixed frequencies are plotted against temperature in **Fig. 7**.

It is observed that at fixed frequency, the ε′ value increases non-linearly with increase of temperature and this increase is relatively stronger at low frequency (e.g., 100 Hz, where the ε′ values are comparatively high) as compared to that of high frequency (e.g., 1 MHz, where the ε′ values are low). The interfacial polarization effect and dc conductivity contribution are the facts for relatively higher increase of ε′ values at low frequencies with the increase of temperature of the PNC film.

The relaxation peak of PVA local chain motion shifts to higher frequencies with increasing temperature in both the ε″ and tanδ spectra (**Fig. 6**), since thermal agitation enhances the free volume within the material which favours to facilitate the orientation of polar segments of PVA chain. Further, it is observed that there is significant increase in the height of tanδ relaxation peak with the increase of temperature of the film. The relaxation time of chain segmental dynamics is determined from the frequency f_p value corresponding to the relaxation peak using the relation $\tau = (2\pi f_p)^{-1}$. It is found that the τ_ε (relaxation time evaluated from ε″ peak) is higher than that of the $\tau_{tan\delta}$ (relaxation time evaluated from tanδ peak), which is common behaviour of these relaxations in polymeric nanocomposites [**6–8**].

The temperature dependent M' and M'' spectra of PVA–3 wt% ZnO film are shown in **Fig. 8**. Similar to the temperature dependent behaviour of ε″ and tanδ peaks, the M'' peak also shifts towards higher frequency region and its height increases with the increase of temperature. The relaxation time τ_M is also determined using the frequency value f_m corresponding to the M'' peak. Interestingly, in addition to PVA α-relaxation, the M'' spectra also exhibit a lower frequency relaxation peak at 60 °C which is attributed to the MWS relaxation process. This peak is appeared in the frequency range of our measurements at higher temperature owing to shift of the spectra towards high frequency region as the temperature of film increases. This MWS relaxation peak found at 60 °C in low frequency region also confirms that there is MWS relaxation peak at lower temperatures but it is below 20 Hz.

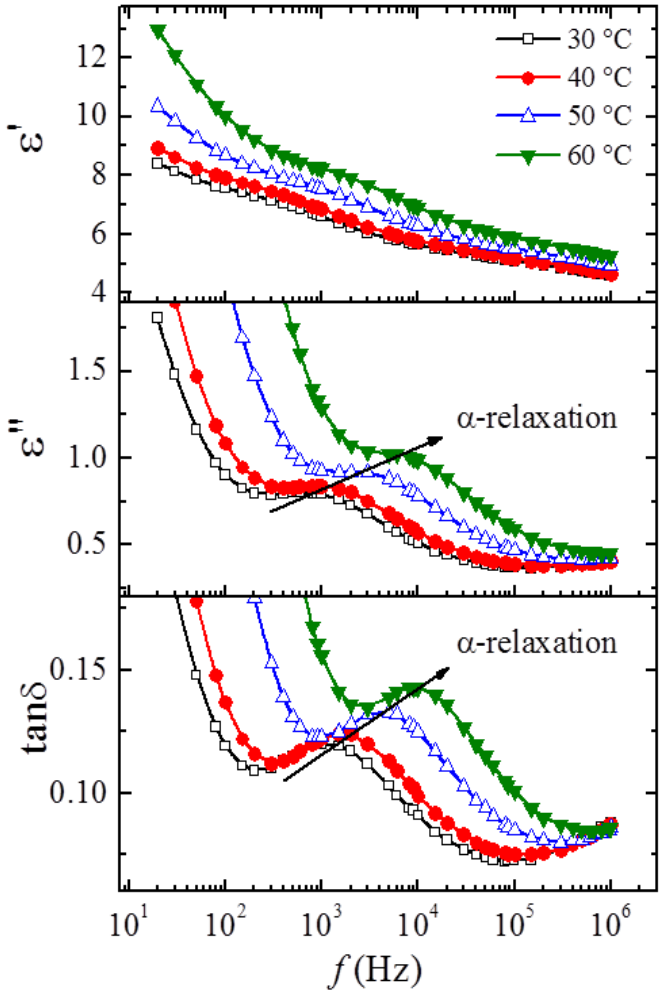

Fig. 6. Frequency dependent real part ε′ and loss part ε″ of the complex dielectric function, and loss tangent tanδ of PVA–3 wt% ZnO nanocomposite film at different temperatures.

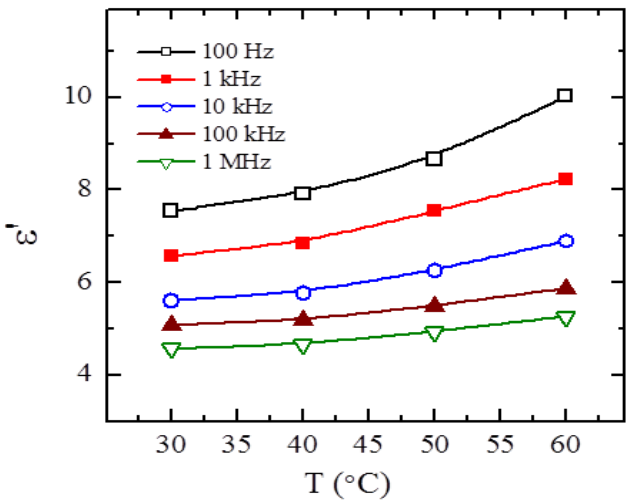

Fig. 7. Temperature dependent ε′ values of PVA–3 wt% ZnO nanocomposite film.

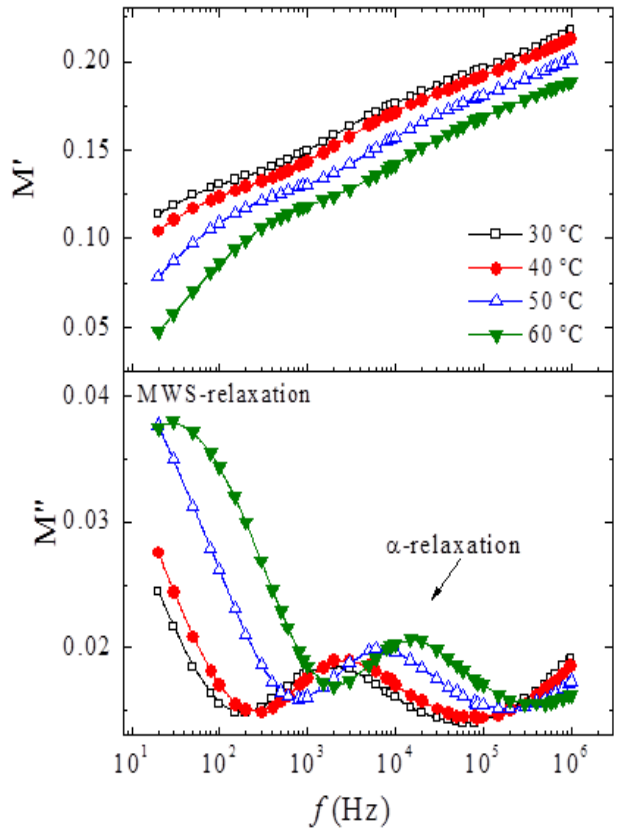

Fig. 8. Frequency dependent real part M' and loss part M'' of complex electric modulus of PVA–3 wt% ZnO nanocomposite film at different temperatures.

In **Fig. 9**, the ε″, tanδ and M'' spectra of PVA–3 wt% ZnO nanocomposite film at 60 °C are plotted simultaneously on the same frequency scale. It is found that the relaxation peak frequency in these spectra has the order $f_\varepsilon < f_{\tan\delta} < f_M$; although they are representing the same relaxation process (α-relaxation) of PVA. This type of shifting behaviour of relaxation peak in different dielectric formalism spectra is also observed for PVA based other nanocomposites **[6,32]**. Further, the appearance of α-relaxation peak is more intense and highly distinguishable which is due to the suppression of other unwanted polarization processes in the electric modulus formalism. Therefore, these comparative results also confirm that the analysis of electric modulus spectra provide more clear information about the relaxation process associated with structural dynamics in the PNC materials.

The Arrhenius behaviour of the relaxation times τ_ε, $\tau_{\tan\delta}$ and τ_M of the PVA–3 wt% ZnO nanocomposite film is shown inupper layer of **Fig. 10**. The activation energy E_τ for polymer segmental motion was calculated using the Arrhenius equation $\tau = \tau_0 \exp(E_\tau/kT)$. The E_τ values were found 0.69 eV, 0.67 eV and 0.66 eV from the inverse of temperature dependent τ_ε, $\tau_{\tan\delta}$ and τ_M plots, respectively. These E_τ values are nearly same confirming that although there is difference in relaxation time values of the same relaxation process when determined from the spectra of different formalism (ε″, tanδ and M''), but the activation energy of this relaxation process is independent of these spectra.

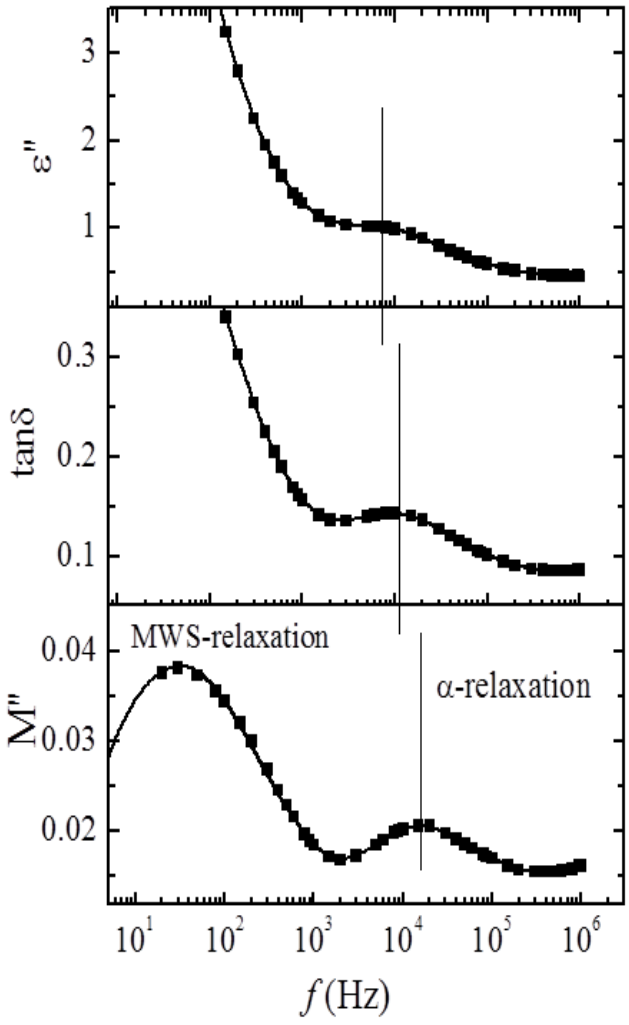

Fig. 9. Simultaneous representation of ε″, tanδ and M'' spectra of PVA–3 wt% ZnO nanocomposite film at 60 °C.

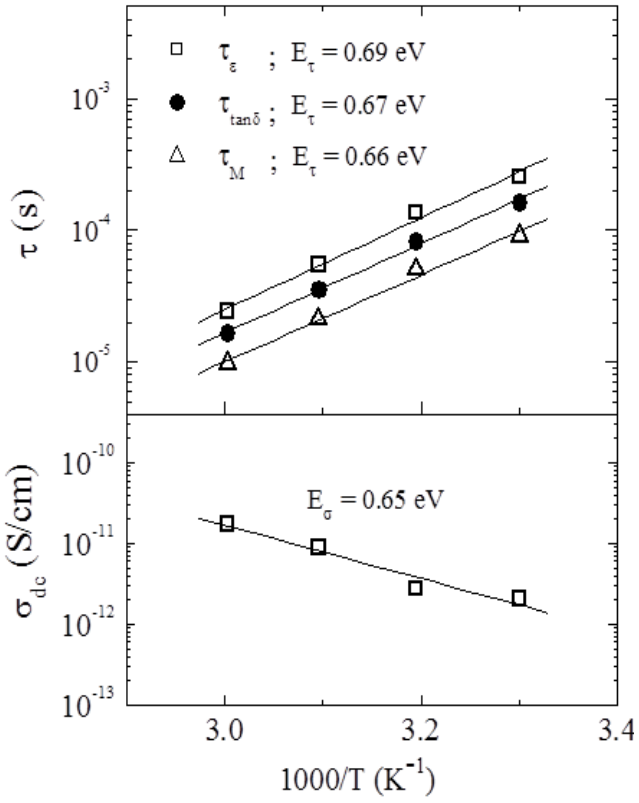

Fig. 10. Arrhenius behaviour of various relaxation times τ and dc conductivity σ_{dc} of PVA–3 wt% ZnO nanocomposite film.

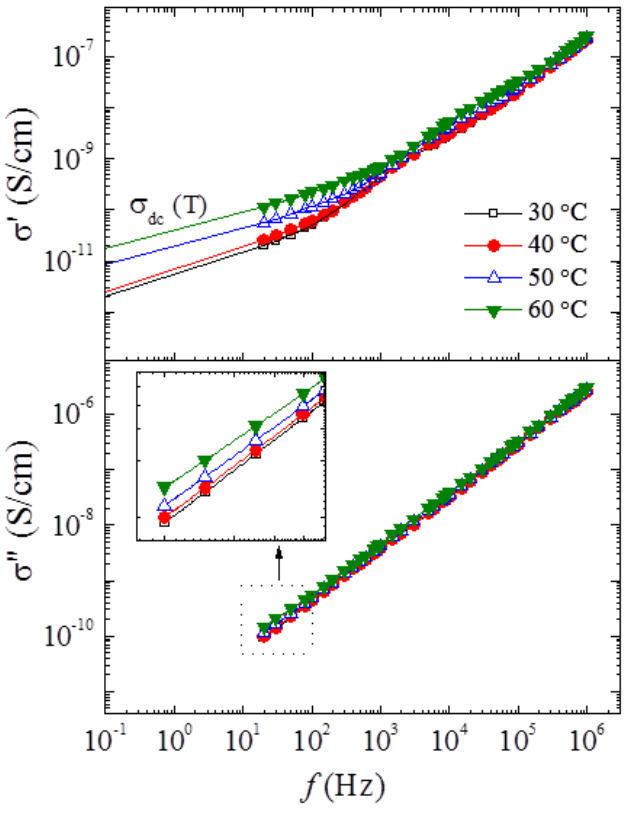

Fig. 11. Frequency dependent real part σ′ and loss part σ″ of the complex ac electrical conductivity of PVA–3 wt% ZnO nanocomposite film at different temperatures. Inset shows the enlarged view of σ″ at low frequencies.

The ac conductivity spectra of PVA–3 wt% ZnO nanocomposite film at different temperatures are depicted in **Fig. 11**. It can be seen from the figure that there is increase of conductivity by about one order of magnitude at lower frequency end of measurements whereas the conductivity change at higher end of frequency is relatively small. The increase in conductivity with increase of temperature confirms the semiconducting behaviour of the nanocomposite film. The dc conductivity contribution at low frequencies is the reason behind it and as the frequency increases, the ac conductivity contribution dominates which shows comparatively weak temperature dependence. The σ″ values of PNC film increase linearly with increase of frequency, at constant temperature. Further, these values also increase with the increase of temperature as shown in enlarged view of the figure.The temperature dependent dc conductivity $\sigma_{dc}(T)$ values of the PVA–3 wt% ZnO film were estimated by interpolation of low frequencies $\sigma'(T)$ spectra as shown by solid lines in **Fig. 11**. The observed σ_{dc} values are plotted against $1000/T$ in the lower layer of **Fig. 10**. This plot revealed that the $\sigma_{dc}(T)$ obeys the Arrhenius behaviour. The conductivity activation energy E_σ of the PVA–3 wt% ZnO film is determined using the Arrhenius relation $\sigma' = \sigma_0 \exp(-E_\sigma/kT)$ and it is found 0.65 eV. The dispersion of ZnO in PVA matrix results in formation of charge transfer ion-dipolar complexes. The same values of E_τ and E_σ for the PNC film confirm that the charge transport mechanism is hopping type and the charges faces same barrier height during transportation as well as relaxation in the dynamical structures of the solid complexes.

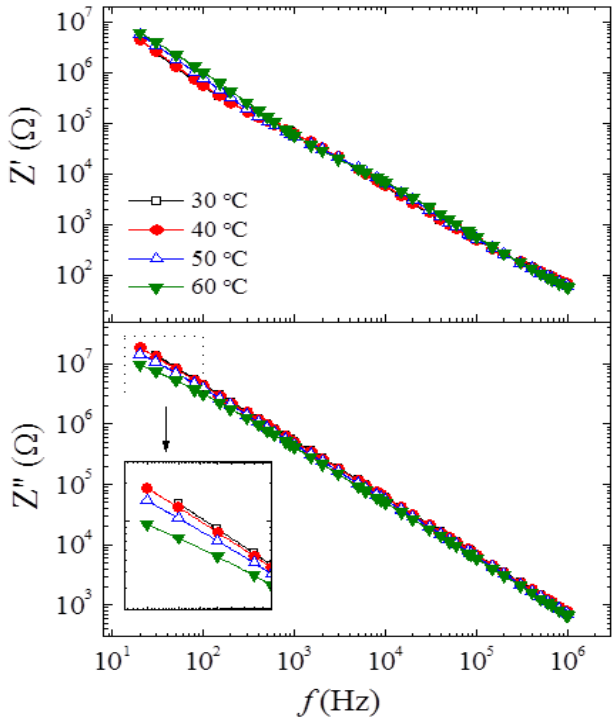

Fig. 12. Frequency dependent real part Z' and reactive part Z'' of complex impedance of PVA–3 wt% ZnO nanocomposite films at different temperatures. Inset shows the enlarged view of Z'' at low frequencies.

The temperature dependent Z' and Z'' spectra of PVA–3 wt% ZnO film are shown in **Fig. 12**. It is observed that the values of Z' and Z'' have gradual decrease by a small amount as the temperature increases, which are shown in enlarged view of the high frequency spectra. These spectra also suggest that the electrical insulation behaviour of the nanocomposite film remains almost same over the temperature variation from 30 to 60 °C.

Conclusions

The dielectric and electrical dispersion behaviour of PVA–ZnO nanocomposites are studied and analyzed in detail by employing different formalisms, namely complex permittivity, electric modulus, complex conductivity and the impedance. The analysis shows that the addition of ZnO nanoparticles in PVA network has significant effect on the dielectric relaxation process of polymer chain segmental dynamics. The relaxation peak corresponding to PVA chain segmental dynamics is observed in dielectric loss and loss modulus spectra of all the nanocomposites, which is not found in case of pristine PVA over the frequency range of experimental measurements. This finding confirms the role of ZnO nanoparticles as PVA chain dynamic exciter in the investigated PNC materials. The real part of permittivity increases anomalously with increase of ZnO concentration up to 5 wt% in the PNCs, whereas at fixed concentration of ZnO it increases non-linearly with increase of temperature. The dc conductivity of these nanocomposite materials also increases anomalously with increase of ZnO concentration. The temperature dependent study of dielectric relaxation time and dc conductivity of PVA–3 wt% ZnO nanocomposite obey the Arrhenius behaviour, having equal values of relaxation and conductivity activation energies. The XRD results confirm the abrupt huge decrease of PVA crystalline phase on inclusion of 1 wt% ZnO nanoparticles which changes little with further increase of ZnO concentration in PVA matrix. The average crystallite size of ZnO nanoparticles is 35 nm and their presence in the PVA chain backbone is observed from the XRD study of the nanocomposites. The dielectric and electrical properties of PVA–ZnO nanocomposites confirm the potential applications of these materials as nanodielectric in electronic and electrical device industries.

Acknowledgements

Authors are grateful to the Department of Science and Technology (DST), New Delhi for providing the experimental facilities through research projects Nos. SR/S2/CMP-09/2002, SR/S2/CMP-0072/2010 and the DST–FIST program. One of the authors SC is thankful to the DST, New Delhi for the award of SERB Fast Track Young Scientist research project No. SR/FTP/PS-013/2012.

References

1. Ray, S. R.; Bousmina, M.; Polymer Nanocomposites and Their Applications; American Scientific Publishers: California, USA, **2006**.
2. Keith, N. J.; Dielectric Polymer Nanocomposites; Springer Science + Business Media, LLC, **2010**. **DOI:** 10.1007/978-1-4419-1591-7
3. Mittal, V.; Characterization Techniques for Polymer Nanocomposites; Wiley-VCH Verlag GmbH & Co. KgaA, **2012**. **DOI:** 10.1002/9783527654505
4. Reddy, B. S. R.; Advances in Nanocomposites - Synthesis, Characterization and Industrial Applications; InTech: Croatia, **2011**.
5. Hmar, J. J. L.; Majumder, T.; Roy, J. N.; Mondal, S. P.; *J. Alloys Comp.*, **2015,***651*, 82–90. **DOI:** 10.1016/j.jallcom.2015.08.101
6. Sengwa, R. J.; Choudhary, S.; Sankhla, S.; *Compos. Sci. Technol.*, **2010,***70*, 1621. **DOI:** 10.1016/j.compscitech.2010.06.003
7. Choudhary, S.; Sengwa, R. J.; *J. Appl. Polym. Sci.*,**2012,***124*, 4847. **DOI:** 10.1002/app.35556
8. Choudhary, S.; Sengwa, R. J.; *Polym. Bull.*, **2015,***72*, 2591. **DOI:** 10.1007/s00289-015-1424-2
9. Bouropoulos, N.; Psarras, G. C.; Moustakas, N.; Chrissanthopoulos, A.; Baskoutas, S.; *Phys. Stat. Sol.(a)*, **2008,** *205*, 2033. **DOI:** 10.1002/pssa.200778863
10. Kinadjian, N.; Achard, M. F.; López, B. J.; Maugey, M.; Poulin, P.; Prouzet, E.; Backov, R.; *Adv. Funct. Mater.*, **2012,***22*, 3994. **DOI:** 10.1002/adfm.201200360
11. Wang, M.; Lian, Y.; Wang, X.; *Curr. Appl. Phys.*, **2009,***9*, 189. **DOI:** 10.1016/j.cap.2008.01.009
12. Bai, Z.; Yan, X.; Chen, X.; Liu, H.; Shen, Y.; Zhang, Y.; *Curr. Appl. Phys.*, **2013,***13*, 165. **DOI:** 10.1016/j.cap.2012.07.005
13. Fernandes, D. M.; Winkler Hechenleitner, A. A.; Lima, S. M.; Andrade, L. H. C.; Caires, A. R. L.; Gómez Pineda, E. A.; *Mater. Chem. Phys.*, **2011,***128*, 371. **DOI:** 10.1016/j.matchemphys.2011.03.002
14. Im, Y. M.; Oh, T. H.; Nathanael, J. A.; Jang, S. S.; *Mater. Lett.*, **2015,***147*, 20. **DOI:** 10.1016/j.matlet.2015.02.004
15. Tamgadge, Y. S.; Sunatkari, A. L.; Talwatkar, S. S.; Pahurkar, V. G.; Muley, G. G.; *Opt. Mater.*, **2016,***51*, 175. **DOI:** 10.1016/j.optmat.2015.11.037
16. Roy, A. S.; Gupta, S.; Sindhu, S.; Parveen, A.; Ramamurthy, P. C.; *Composites: Part B*, **2013,***47*, 314. **DOI:** 10.1016/j.compositesb.2012.10.029
17. Chandrakala, H. N.; Ramaraj, B.; Shivakumaraiah, Lee, J. H.; Siddaramaiah, *J. Alloys Compd.*, **2013,***580*, 392. **DOI:** 10.1016/j.jallcom.2013.06.091
18. Vaishnav, D.; Goyal, R. K.; *IOP Conf. Series: Mater. Sci. Eng.*, **2014,***64*, 012016. **DOI:** 10.1088/1757-899X/64/1/012016
19. Rashmi, S. H.; Raizada, A.; Madhu, G. M.; Kittur, A. A.; Suresh, R.; Sudhina, H. K.; *Plastics, Rubber Compos.*, **2015,***44*, 33. **DOI:** 10.1179/1743289814Y.0000000115
20. Karthikeyan, B.; Pandiyarajan, T.; Mangalaraja, R. V.; *Spectrochim. Acta Part A*, **2016,***152*, 485. **DOI:** 10.1016/j.saa.2015.07.053
21. Fernandes, D. M.; Winkler Hecjenleitner, A. A.; Lima, S. M.; Andrade, L. H. C.; Caires, A. R. L.; Gómex Pineda, E. A.; *Mater. Chem. Phys.*, **2011,***128*, 371. **DOI:** 10.1016/j.matchemphys.2011.03.002
22. Van Etten, E. A.; Ximenes, E. S.; Tarasconi, L. T.; Garcia, I. T. S.; Forte, M. M. C.; Boudinov, H.; *Thin Solid Films*, **2014,***568*, 111. **DOI:** 10.1016/j.tsf.2014.07.051
23. Rao, J. K.; Raizada, A.; Ganguly, D.; Mankad, M. M.; Satayanarayana, S. V.; Madhu, G. M.; *J. Mater. Sci.*, **2015,***50*, 7064. **DOI:**10.1007/s10853-015-9261-0
24. Hassan, C. M.; Peppas, N. A.; *Adv. Polym Sci.*, **2000,***153*, 37. **DOI:** 10.1007/3-540-46414-X_2

25. Kokabi, M.; Sirousazar, M.; Hassan, Z.; *Eur. Polym. J.*, **2007,***43*, 773.
DOI: 10.1016/j.eurpolymj.2006.11.030
26. Scotchford, C. A.; Cascone, M. G.; Downes, S.; Giusti, P.; *Biomaterials*, **1998,***19*, 1.
DOI: 10.1016/S0142-9612(97)00236-6
27. Han, S.; Huang, W.; Shi, W.; Yu, J.; *Sensors and Actuators B*, **2014,** *203*, 9.
DOI: 10.1016/j.snb.2014.06.083
28. Morales-Acosta, M. D.; Quevedo-López, M. A.; Ramírez-Bon, R.; *Mater. Chem. Phys.*, **2014,***146*, 380.
DOI: 10.1016/j.matchemphys.2014.03.042
29. Sengwa, R. J.; Choudhary, S.; *J. Phys. Chem. Solids*, **2014,***75*, 765–774.
DOI: 10.1016/j.jpcs.2014.02.008
30. Choudhary, S.; Sengwa, R. J.; *J. Appl. Polym. Sci.*, **2014,***131*, 40617.
DOI: 10.1002/app.40617
31. Irimpan, L.; Nampoori, V. P. N.; Radhakrishnan, P.; *J. Appl. Phys.*, **2008,** *104*, 113112.
32. Choudhary, S.; Sengwa, R. J.; *Express Polym. Lett.*, **2010,***9*, 559.
DOI: 10.3144/expresspolymlett.2010.70
33. Tantis, I.; Psarras, G. C.; Tasis, D.; *Express Polym. Lett.*, **2012,***6*, 283.
DOI: 10.3144/expresspolymlett.2012.31
34. Sinha, S.; Chatterjee, S. K.; Ghosh, J.; Meikap, A. K.; *Polym. Compos.*, **2017,**38, 287**..**
DOI: 10.1002/pc.23586

